ORIGINAL ARTICLE

Sensitivity of 3D thermal models to the choice of boundary conditions and thermal properties: a case study for the area of Brandenburg (NE German Basin)

Vera Noack · Magdalena Scheck-Wenderoth · Mauro Cacace

Abstract Based on newly available data of both, the structural setting and thermal properties, we compare 3D thermal models for the area of Brandenburg, located in the Northeast German Basin, to assess the sensitivity of our model results. The structural complexity of the basin fill is given by the configuration of the Zechstein salt with salt diapirs and salt pillows. This special configuration is very relevant for the thermal calculations because salt has a distinctly higher thermal conductivity than other sediments. We calculate the temperature using a FEMethod to solve the steady state heat conduction equation in 3D. Based on this approach, we evaluate the sensitivity of the steady-state conductive thermal field with respect to different lithospheric configurations and to the assigned thermal properties. We compare three different thermal models: (a) a crustal-scale model including a homogeneous crust, (b) a new lithosphere-scale model including a differentiated crust and (c) a crustal-scale model with a stepwise variation of measured thermal properties. The comparison with measured temperatures from different structural locations of the basin shows a good fit to the temperature predictions for the first two models, whereas the third model is distinctly colder. This indicates that effective thermal conductivities may be different from values determined by measurements on rock samples. The results suggest that conduction is the main heat transport mechanism in the Brandenburg area.

Keywords Conductive thermal field · 3D thermal model · Lithosphere–asthenosphere boundary · Zechstein salt · Brandenburg · Northeast German Basin

Introduction

Large-scale 3D thermal models are useful in the planning state of geothermal production sites, as they provide comprehensive information about structural heterogeneities and their relevance for the thermal field in potential exploitation areas.

We present new results from 3D thermal modelling in the area of Brandenburg in north-eastern Germany (Fig. 1a) based on a recently published structural model (Noack et al. 2010) of the basin fill with an improved representation of the salt structures.

The study area is located in the south-eastern part of the Northeast German Basin (NEGB) within the Central European Basin System. As the formation of the basin started with extensive volcanism in the Late Carboniferous/Early Permian the lowermost geological unit of the basin fill is composed of volcanic rocks (Benek et al. 1996). Above the volcanic rocks, the Permian to Cenozoic sediment fill attains a thickness of up to 8,000 m in the central part of the NEGB (Schwab 1985; Scheck and Bayer 1999). The structural setting in the basin is mainly influenced by a layer of strongly mobilised Upper Permian Zechstein salt. Reconstructions of the initial thickness of the Zechstein salt indicate the highest thickness of up to 2,500 m in the north-western basin centre, but halokinetic movements generated

V. Noack · M. Cacace
University of Potsdam, Am Neuen Palais 10,
14469 Potsdam, Germany
e-mail: Mauro.Cacace@gfz-potsdam.de

V. Noack (✉) · M. Scheck-Wenderoth · M. Cacace
Helmholtz Centre Potsdam, GFZ German Research Centre
for Geosciences, Telegrafenberg, 14473 Potsdam, Germany
e-mail: Vera.Noack@gfz-potsdam.de

M. Scheck-Wenderoth
e-mail: leni@gfz-potsdam.de

Fig. 1 **a** Location of study area with topography in UTM Zone 33N (ETOPO1, after Amante and Eakins, 2009) of Central Europe. Large *red rectangle* encloses the area covered by the 3D thermal models of Brandenburg, *black line* delineates the border of Brandenburg. **b** Top of the Zechstein salt for the model area with location of wells where measured temperatures are available. Coordinates are Gauss Krüger zone 4. *Black line* indicates the location of a representative, NNE–SSW oriented cross section which cuts major geological structures across the model
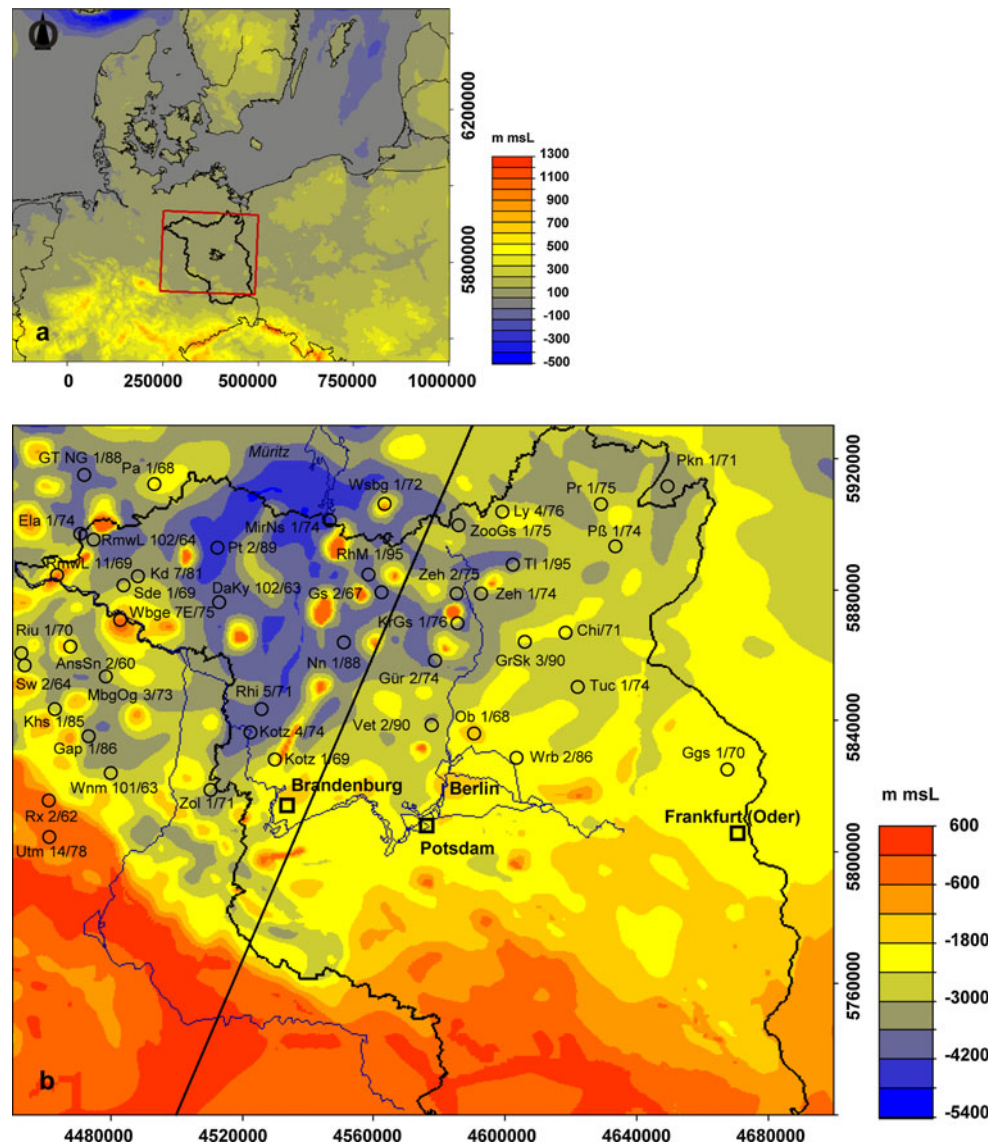
local structures such as salt pillows and salt diapirs, where much larger thicknesses occur (Scheck et al. 2003). Also, the deep structure of the basin is differentiated, as the sediments are underlained by crustal domains that have different consolidation ages (Maystrenko and Scheck-Wenderoth 2011).

Accordingly, the structural setting of the modelled area in Brandenburg is highly complex (Fig. 1b). In the northwest, the area comprises a part of the basin centre of the NEGB, where the base of the Permian–Cenozoic basin fill reaches depths of more than 8,000 m (Noack et al. 2010). In the south, the inverted southern margin of the basin is included, where the crystalline crust comes close to the surface. In the basin area, the structural setting is mainly determined by the configuration of the Zechstein salt, which is characterised by numerous salt pillows and diapirs, surrounded by areas where the salt has been withdrawn.

Diapirs piercing their overburden reach structural amplitudes of up to 4,500 m (Noack et al. 2010). These salt structures are surrounded by salt rim synclines of various Mesozoic and Cenozoic ages. The largest of these rim synclines are of Tertiary age and filled with up to 2,000 m thick clastic sediments (Noack et al. 2010).

The geothermal field of the NEGB and thus also the area of Brandenburg have been investigated with different focus and on different scales during the last 50 years. Initial studies of the surface heat flow density in the area of Brandenburg have already been carried out by Schössler and Schwarzlose (1959). These studies were followed by investigations on the relationship between the thermal field and the deep structural setting in northern Germany (e.g. Hurtig 1975; Hurtig and Oelsner 1979). Maps of the surface heat flow density and temperature maps at different depths have been provided by Hurtig et al. (1992) for entire

Europe. According to these maps, a large positive anomaly in heat flow stretches from Poland to the river Elbe, crossing the area of Berlin. Also published temperature maps at 1,000 and 2,000 m depth indicate high temperature anomalies related to areas in the north-west and south-west of Brandenburg. These published maps of temperature and heat flow were based on interpretations of corrected temperatures, measured by continuous thermal logging in wells. Beer (1996) presented a temperature map covering the area of Brandenburg and proposed a tentative empirical correction method for temperature measurements, later improved by Förster (2001). In this way, a new thermal database for the NEGB was provided, additionally including data of both thermal conductivity and radiogenic heat production determined on drill cores and well-logs (Norden and Förster 2006; Norden et al. 2008; Fuchs and Förster 2010).

Already Ollinger et al. (2010) pointed out that calculations of the thermal field are most sensitive to the variations in thermal conductivity. They conclude this from sensitivity analyses for thermal conductivities in the sedimentary layers assuming a constant basal heat flow of 60 mW/m^2 for the geothermal site Groß Schönebeck in NE Germany.

In addition, the relationship between the structural setting and the thermal field within the NEGB has been investigated by large-scale thermal models based on 3D Finite Element simulations (Bayer et al. 1997; Scheck 1997). Assuming a homogeneous crust down to 30 km depth and a heat flow of 25 mW/m^2 as lower boundary condition at the base of the crust, these models were able to reproduce the generalised pattern of the temperature distribution in the temperature maps published earlier (Hurtig et al. 1992). These works focussed on the effect of alternative lower boundary conditions. They compared the resulting thermal field for a fixed temperature of 600°C and a fixed heat flow of 25 mW/m^2 at the crust mantle boundary (Moho). Concerning the structural setting of the basin fill these models also included the Zechstein salt, though with a limited horizontal resolution of 4 km (Bayer et al. 1997; Scheck 1997; Ondrak et al. 1998). However, these models already demonstrated that the salt structures control the short-wavelength pattern of heat flow as well as of the temperature distribution. In the shallow part of the basin, a more recent 3D thermal model with an improved resolution of 1 km has assessed this influence for the present-day thermal field of Brandenburg (Noack et al. 2010). The improved representation of the salt structures allowed to evaluate the influence of structural heterogeneities on the temperature distribution. Due to the specific configuration of the salt diapirs and their surrounding clastic sediments and carbonates a phenomenon in the temperature-distribution can be observed which is known

as "chimney effect". This effect occurs due to the interaction between the thermally highly conductive Zechstein salt and the low conductive clastic rocks. Thereby, the highly conductive salt efficiently transports the heat to the surface within the salt diapirs, whereas the neighbouring lower conductive clastics and carbonates act as insulating layers. This leads to cooling effects within and below the salt. In contrast, the thick low conductive sediments act as a thermal blanket and cause the storage of heat below. The result is a very characteristic temperature distribution around the salt structures. Compared to the neighbouring insulating layers, the 3D thermal model predicts higher temperatures at the same depth in the top region of the diapirs and lower temperatures within and below. This modelling result is confirmed by observed temperatures as for example at the diapir Kootzen in Brandenburg (Beer and Hurtig 1999).

Other studies focussed on the base of the lithosphere–asthenosphere boundary (LAB) as lower boundary condition. It is generally assumed that the base of the lithosphere is represented by the 1,300°C isotherm, at which partial melting of peridotite occurs (Turcotte and Schubert 2002). To constrain the depth and geometry of the LAB Cacace and Scheck-Wenderoth (2010) tested different seismological models. Maystrenko and Scheck-Wenderoth (2011) developed a lithospheric configuration for the entire Central European Basin System that is consistent with temperature and gravity observations. Apart from that, Norden et al. (2008) investigated the sensitivity of the thermal field in the NEGB with respect to different configurations of the lithosphere. All these earlier studies provided basic results to investigate the main controlling factors on the 3D thermal field.

Newly available data of both, the structural setting of the deeper lithosphere of Brandenburg and of thermal rock properties measured in wells of the NEGB, enabled us to better constrain thermal models. The new aspects of this paper concern the validation of earlier models in that we address the sensitivity of our results with regard to specific controlling factors of the 3D conductive field. These are the lithosphere configuration and the chosen boundary conditions, as well as the chosen thermal properties of the geological units. Thus, this approach permits to estimate to which degree specific assumptions for the configuration of the deeper lithosphere and as well as for the thermal properties influence the pattern of the conductive thermal field. Moreover, we address the thermal interaction between different crustal configurations and the sedimentary overburden and their effects on heat transport within the basin. Besides of this our systematic analysis reveals if the assumption of dominantly conductive heat transport is generally valid or if areas exist where this assumption is inconsistent with observations.

We focus on the 3D conductive thermal field using a finite element method (FEM) and assume steady-state conditions for the model area. To evaluate the sensitivity of our 3D conductive thermal model with respect to different parameters, we run a series of simulations of which we present three different thermal models as end member scenarios. Thereby, the configuration of the lithosphere is the first parameter addressed, followed by an evaluation of the influence of different thermal properties. To validate our model results, we compare modelled temperatures with temperatures observed in 45 wells (Fig. 1b).

Method

Assuming that heat moves predominantly by conduction through the lithosphere (Fowler 1996), we assess the regional thermal field by solving the three-dimensional equation of heat conduction (Bayer et al. 1997). Ignoring temperature and pressure dependence of the coefficients, the principle equation is:

$$c\rho(\delta T/\delta t) = \mathrm{div}(\lambda \mathrm{grad}\ T) + S$$

(where c is heat capacity, ρ is density, T is temperature, λ is thermal conductivity, gradT is the temperature gradient, t is time, and S is radiogenic heat production). Furthermore, we assume an equilibrium situation for the model area and calculate the temperature by solving numerically the conductive heat equation for steady-state conditions ($\delta T/\delta t = 0$):

$$0 = \mathrm{div}(\lambda \mathrm{grad}\ T) + S$$

using a 3D FEM (Bayer et al. 1997). Thus, the temperature distribution does not depend on heat capacity and density, but is sensitive to the values of the thermal parameters thermal conductivity (λ) and radiogenic heat production (S) as well as to the choice of boundary conditions. In consequence of the stationary approach, the system of linear equations is solved iteratively until the stationary solution is achieved. The FEM is based on the conjugated gradient solver with an iteration limit of $1.e-5$. The model units are discretized as deformed eight-noded prisms with a grid resolution of 1 km and 250×210 grid points in horizontal direction. The vertical length of the elements corresponds to the thickness of the layers. For the temperature calculations, we use the software Geological Modelling System (GMS, developed at GFZ Potsdam, Bayer et al. 1997).

As upper boundary condition we assign a fixed temperature of 8°C at the surface, which corresponds to the average annual surface temperature in the area. The lateral boundaries are considered closed. We use the 3D structural model of Brandenburg (Noack et al. 2010) as a starting point for the calculations of the temperature field. This model comprises an area of 250×210 km horizontally with a horizontal resolution of 1 km and extends downward to the top pre-permian surface. The vertical resolution of the model is defined by the number of layers resolved in the model. The model integrates 11 layers of the basin fill (Fig. 2a) consisting from top to bottom of: Quaternary, Tertiary, Upper Cretaceous, Lower Cretaceous, Jurassic, Triassic Keuper, Triassic Muschelkalk, Triassic Buntsandstein, Permian Zechstein, Permian Rotliegend (post-volcanic) and Permo-Carboniferous Volcanics.

As mentioned above, the structural setting in the basin fill is controlled by the distribution of the Zechstein salt. This concerns both the configuration of the highly irregular top salt surface as well as of the base of the salt. At the south-western basin margin, the pre-Zechstein basement is uplifted by about 5 km south of the Gardelegen fault (Scheck-Wenderoth et al. 2008). Apart from this area, the base of the Zechstein salt is a comparatively flat surface, which reaches up to 5,000 m depth in its deepest part in the north-west (Fig. 2b). This north-western part of the model is characterized by the most mature salt diapirs and by areas of close-to zero present-day thickness of the salt where salt has been removed (Fig. 2c). The structural configuration of the basin fill is the same for all thermal models in this study.

For the temperature calculation, we assign lithology-dependent physical properties constant to each stratigraphic unit of the model depending on the dominant lithology of the respective units (Table 1).

The thermal model 1 reaches downward to the crust-mantle boundary (Moho) and integrates a homogeneous layer for the pre-permian crust. For this model, a basal heat flow of 30 mW/m² at the Moho is adopted as lower boundary condition following earlier studies (Noack et al. 2010).

For the new thermal model 2, we change the lower boundary condition by extending the model downward to the lithosphere–asthenosphere boundary (LAB) and by considering a differentiated crust.

Here a fixed temperature of 1,300°C is assumed as lower boundary condition at the base of the LAB (Turcotte and Schubert 2002; Scheck-Wenderoth and Maystrenko 2008).

For both models, we assign the same thermal properties after Bayer et al. (1997) for the Permian to Cenozoic units.

In thermal model 3, we use the same configuration of the crust and thus the same lower boundary condition of 30 mW/m² at the Moho as used for model 1, but assign measured thermal properties after Norden and Förster (2006), Norden et al. (2008) and Fuchs and Förster (2010) for the respective units.

The models differ according to the characteristics presented in Table 2. As mentioned before, we use the same

Fig. 2 **a** 3D view on the structural configuration of the Permian to Cenozoic basin fill with colour key for the stratigraphic units differentiated in the model. **b** Base of Permian Zechstein salt (modified after Noack et al. 2010). **c** Thickness of Permian Zechstein salt (modified after Noack et al. 2010). **d** Depth of the crust–mantle boundary of the crustal-scale thermal model
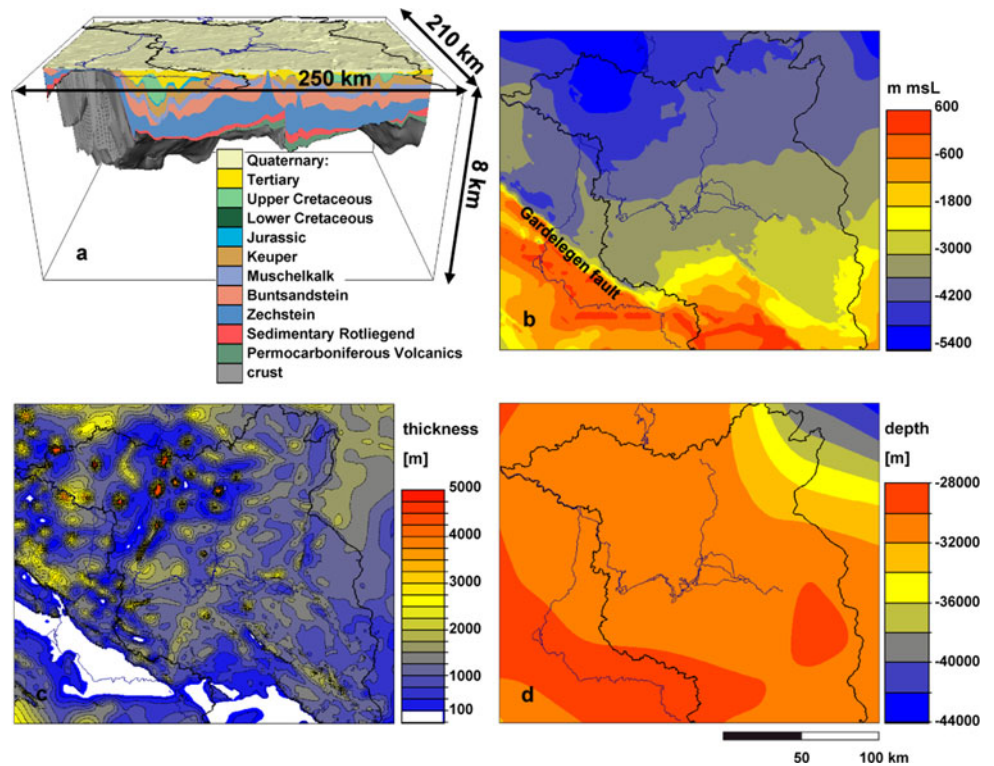

Table 1 Assigned physical properties for geothermal modelling: for the lithological characteristics dominant lithology is mentioned first

Stratigraphic unit	Lithology	λ (W/m K) Model 1, 2	S (W/m^3) Model 1, 2	λ (W/m K) Model 3	S (W/m^3) Model 3
Quaternary	Sand, Silt and Clay	1.50	0.70e−6	1.80[c]	0.9e−6[a]
Tertiary	Sand, Silt and Clay	1.50	0.70e−6	1.80[c]	0.9e−6[a]
Upper Cretaceous	Limestone (Chalk)	1.90	0.30e−6	3.04[b]	0.6e−6[a]
Lower Cretaceous	Clays with Sand and Silt	2.00	1.40e−6	2.71[b]	1.5e−6[a]
Jurassic	Clays with Sand, Silt and Marl	2.00	1.40e−6	2.71[b]	1.5e−6[a]
Keuper	Clays with Marl and Gypsum	2.30	1.40e−6	2.35[b]	1.6e−6[a]
Muschelkalk	Limestone	1.85	0.3e−6	2.30[b]	1.0e−6[a]
Buntsandstein	Silts with Sand, Clay and Evaporite	2.00	1.00e−6	2.58[b]	1.8e−6[a]
Zechstein	Evaporites	3.50	0.09e−6	4.50[c]	0.4e−6[a]
Sedimentary Rotliegend	Clay-, Silt- and Sandstone	2.16	1.00e−6	3.30[a]	1.4e−6[a]
Permo-Carboniferous Volcanics	Rhyolithe and Andesite	2.50	2.0e−6	2.50[a]	2.6e−6[a]

Stratigraphic unit	Lithology	λ (W/m K) Model 1,3	S (W/m^3) Model 1,3
Crustal configuration			
Homogenous	Granite to Granodiorite	2.55	1.5e−6

Stratigraphic unit	Lithology	λ (W/m K) Model 2	S (W/m^3) Model 2
Differentiated			
Pre-permian	Strongly compacted clastics	2.65	1.5e−6
Upper crust	Granites	3.10 (2.70)	2.5e−6 (2.0)
Lower crust	Gabbro	2.70 (2.30)	0.8e−6 (0.6)
Lithospheric mantle	Peridotite	3.95	0.03e−6

Values for the thermal properties are assigned following earlier studies for model 1 and model 2 after Bayer et al. (1997). Measured values used for model 3: [a]radiogenic heat production and thermal conductivity data after Norden and Förster (2006), [b]thermal conductivity data after Fuchs and Förster (2010) and [c]after Norden et al. (2008); additional input thermal properties used for the differentiated lower lithosphere of model 2; thermal properties for the pre-permian after Bayer et al. (1997); for the upper crust and the lower crust after Norden et al. (2008) and for the lithospheric mantle after Scheck-Wenderoth and Maystrenko (2008)

Table 2 Summary of the characteristics for the calculated models

Model	Thermal properties of sediments	Crustal structure	Boundary conditions	
1	After Bayer et al. (1997)	Homogenous	Moho	30 mW/m²
2	After Bayer et al. (1997)	Differentiated	LAB	1,300°C
3	Measured thermal properties	Homogenous	Moho	30 mW/m²

structural configuration of the basin fill for all models. Likewise, the upper boundary is fixed for all models with an average annual surface temperature of 8°C at the surface. Because of that, model 2 differs from models 1 and 3 in both their lower boundary condition and their composition of the lithosphere.

To validate our model results a database including 84 temperature measurements (Tables 3, 4) is available for the area of Brandenburg (Förster 2001; Norden et al. 2008). This database offers (1) temperatures at total depth from the equilibrium temperature logs, (2) temperatures corrected at total depth of perturbed temperature logs and (3) corrected Bottom-Hole Temperatures. As can be seen in Tables 3 and 4, the temperatures originate from different wells and reach various depths and stratigraphic levels. Figure 1b shows the lateral distribution of these wells displayed on the top of the salt surface and illustrates their position with respect to different structural elements across the model area. Some of the measurements have been made within the deepest part of the basin in the north-west, but also in areas where the salt has partly been removed. Moreover, observations were also available at the basin margins in the south-west and in the east.

Results

Different configurations of the lithosphere

For the lithosphere below the Paleozoic to Cenozoic deposits, we test two different configurations. In model 1, the pre-permian crust is defined by a homogeneous layer of granitic to granodioritic composition (Table 1) which is limited downward by the Moho. The shallowest position for the Moho is observed at ~30 km depth at the south-western basin margin (Fig. 2d), where the sub-Permian is thickest and comes close to the surface. From there, the Moho descends gently northward across the basin. In the north-eastern edge of the model, the Moho deepens considerably to 40 km depth. The crust itself is characterized by a very large volume with a higher thermal conductivity and a higher radiogenic heat production than the sediments and thus also mimics the heat input of the crystalline crust (Table 1).

For model 2, newly available data describing the configuration of the deeper lithosphere in the area permitted to define a more realistic lithosphere-scale model (Maystrenko and Scheck-Wenderoth 2011). The latter is based on deep seismic experiments and constrained by 3D gravity modelling. Accordingly, the depth level of both an improved Moho and the lithosphere–asthenosphere boundary (LAB) are integrated.

Moreover, the crystalline crust is differentiated into a layer of pre-permian sediments, an upper layer of silicic composition and a lower layer of mafic composition. Thus, the new lithosphere-scale structural model integrates additional layers for the pre-permian, the upper crust, the lower crust and the Upper Mantle downward to the LAB. For the refined lithospheric part, we assign in the same way thermal properties (Table 1) corresponding to their main lithologies. These are taken for the upper crust and the lower crust after Norden et al. (2008); for the pre-permian after Scheck (1997) and for the lithospheric mantle after Hofmeister (1999) and Scheck-Wenderoth and Maystrenko (2008). According to its granitic composition, the thermal conductivity of the upper crust is distinctly higher than that of the sediments. Additionally, the radiogenic heat production is nearly three times higher than that for the lower crust. This crustal contribution in concert with the crustal configuration strongly controls the heat input from the crust.

The thickness of the upper crust in model 2 (Fig. 3a) increases rapidly from less than 6 km in the north-western part of the model to ~24 km in the south-east. The largest thickness (up to 30 km) is reached at the basin margin in the south-west. This configuration is important for the temperature calculation as the granites of the upper crust produce large amounts of radiogenic heat (Table 1).

A complementary pattern to the thickness of the upper crust is visible for the underlying lower crust (Fig. 3b). The lower crust is thickest (with up to 20 km) in the north-western part of the model, whereas the thickness of this layer decreases to less than 4 km to the south and the east.

Similar to model 1, the shallowest position for the new Moho is observed at ~30 km depth at the south-western basin margin (Fig. 3c). Towards the basin, the Moho descends in a NNW–SSE oriented depression, rises up and descends again in the north-eastern edge of the model.

The LAB as the lowermost boundary of the model reaches a depth of ~120 km in the western part, and descends with a gentle gradient to ~140 km in the north-eastern part (Fig. 3d) of the model. The lithosphere mantle

Table 3 Observed temperatures in wells used for model validation: T at total depth (TD) of temperature log, for perturbed logs corrected temperature at TD of log and corrected bottom-hole temperatures after Förster (2001)

Well	TD of log/depth of BHT (m)	T at TD of log (°C)	Tcorr. at TD of log (°C)	BHT corr. (±3°C)	BHT corr. (±10°C)	T of model 2 (°C)
AnsSn/Arendsee 2/60	1,500	69.8				77
Chi/Chorin 1/71	3,800	144.3	147			146
DaKy/Dannenwalde 102/63	1,250	49.8				60
Ela/Eldena 1/74	5,150	169.8	181			190
Gap/Garlipp 1/86	4,580	149.7	156			169
Ggs/Gorgast 1/70	3,250	120.8	124			129
Gs/Gransee 2/67	5,050	181.9				186
Gür/Grüneberg 2/74	4,100	157	161			165
Khs/Kahrstedt 1/85	2,300	105				104
Kd/Karstädt 7/81	900	43.4	45			49
Kotz/Kotzen 1/69	4,450	144.4	150			159
Kotz/Kotzen 4/74	5,500	172.6	181			198
KrGs/Kraatz 1/76	4,350	162	168			169
Ly/Lychen 4/76	4,700	154.7	163			167
MbgOg/Meseberg 3/73	4,100	148	151			149
MbgOg/Meseberg 3/73	4,950				173	177
MirNs/Mirow 1/74	4,400	149.2	154			148
MirNsMirow 1/74	6,040				205	193
MirNsMirow 1/74	6,820				233	214
Nn/Neuruppin 1/88	2,081	78.9				94
GT NG/Neustadt-Glewe 1/88	2,284	100.5				98
Ob/Oranienburg 1/68	4,200	124	132			156
Pa/Parchim 1/68	6,150	188	200			195
Pkn/Penkun 1/71	4,100	142.6	144			154
Pkn/Penkun 1/71	5,500				189	195
Pß/Polßen 1/74	4,000	143.4	152			148
Pr/Prenzlau 1/75	4,400	151.5	160			159
Pt/Pritzwalk 2/89	2,145	81.1				95
RmwL/Rambow 102/64	1,950	80				88
RmwL/Rambow 11A/69	4,250	139.8				160
RhM/Rheinsberg 1/95	1,600	66.1				75
Rhi/Rhinow 5/71	5,200	179	182			188
Riu/Riebau 1/70	3,500	149.5				139
Rx/Roxförde 2/62	2,850	97	113			114
Sw/Salzwedel 2/64	3,650	142.6	147			144
Sde/Schilde 1/69	2,400	109.5	111			103
Tl/Templin 1/95	1,652	69.3				82
Tuc/Tuchen 1/74	4,250	139.8	147			167
Utm/Uthmöden 14/78	790			35		40
Utm/Uthmöden 14/78	950			40		45
Vet/Velten 2/90	1,650	64.5				82
Wrb/Wartenberg 2/86	1,749	71.9				88
WsbgWesenberg 1/72	4,250	145.5	149			147
WsbgWesenberg 1/72	5,093			184		174
Wbge/Wittenberge 7E/75	5,200	171.2	181			172
Wnm/Wittenmoor 101/63	550	28.2				35
Zeh/Zehdenick 2/75	3,650	139				146

Table 3 continued

Well	TD of log/depth of BHT (m)	T at TD of log (°C)	Tcorr. at TD of log (°C)	BHT corr. (±3°C)	BHT corr. (±10°C)	T of model 2 (°C)
Zeh/Zehdenick 1/74	4,250	159.5	162			170
Zol/Zollchow 1/71	4,100	149.8	161			158
ZooGs/Zootzen 1/75	5,000	165	173			177

Table 4 Observed temperatures in wells used for model validation after Norden et al. (2008)

Well	Depth (m)	Temperature (°C)	Quality	T of model 2 (°C)
GrSk/Groß Schönebeck 3/90	2,800	119.9	Unperturbed	121
	3,770	135.1	Unperturbed	144
	4,230	148.6	Unperturbed	160
	4,286	150.8	Unperturbed	162
Gs/Gransee 2/76	4,100	156.8	Unperturbed	159
	4,150	157.9	Unperturbed	160
	4,200	159	Unperturbed	162
	4,600	170	Unperturbed	174
	4,650	171.1	Unperturbed	175
	4,750	173.2	Unperturbed	178
	4,800	174.8	Unperturbed	180
	5,000	181	Unperturbed	185
RmwL/Rambow 11/A 69	500	36.2	Unperturbed	45
	750	42.3	Unperturbed	52
	1,700	67.6	Unperturbed	79
	1,950	75.2	Unperturbed	86
	3,200	107.3	Unperturbed	122
	3,450	113	Unperturbed	129
	3,500	114.3	Unperturbed	131
Chi/Chorin 1/71	2,900	126.6	Slightly perturbed	123
	3,650	139.8	Slightly perturbed	141
Sw/Salzwedel 2/64	2,850	122.6	Slightly perturbed	123
	3,000	126.5	Slightly perturbed	126
	3,150	129.2	Slightly perturbed	129
	3,250	131.1	Slightly perturbed	131
	3,350	133	Slightly perturbed	134
Gap/Garlipp 1/86	3,400	125	Corrected	135
	3,800	131	Corrected	145
	3,850	131.7	Corrected	147
	4,150	138.2	Corrected	156
	4,200	139.2	Corrected	158
	4,350	142.2	Corrected	162
	4,400	143.7	Corrected	163
	4,500	149.7	Corrected	166

is assumed to consist of peridotite and accordingly is characterized by a lower radiogenic heat production than the crust, but also a relatively high thermal conductivity (Table 1).

To estimate how far these two different configurations of the deeper lithosphere and thus different conditions for the basal heat input, affect the model results we run a sensitivity analysis for both the crustal-scale model 1 and the lithosphere-scale model 2 using thermal properties after Bayer et al. 1997 and compare their results. Since the thermal properties vary within a certain range and no measurements within the deeper lithosphere are possible,
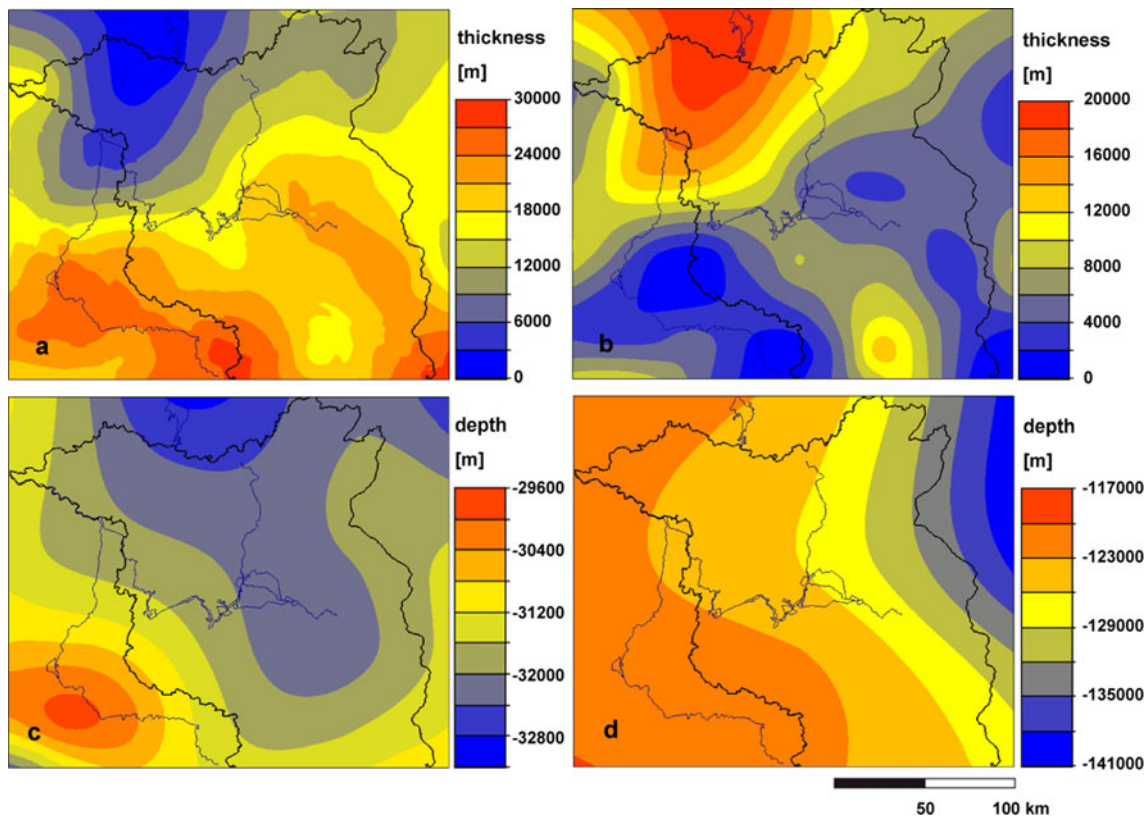
Fig. 3 **a** Thickness of upper crust. **b** Thickness of lower crust. **c** Depth of the crust-mantle boundary of the lithosphere-scale thermal model. **d** Depth of lithosphere–asthenosphere boundary of the lithosphere-scale thermal model

we run sensitivity analyses to estimate the influence of these variations for the crystalline rocks (Table 1, minimum end member values in brackets). A comparison between the crustal-scale model 1 and the lithosphere-scale model 2 allows us to test, how far it is justified to apply a crustal-scale boundary condition, as it is the case if we use a constant heat flow of 30 mW/m^2 at the Moho.

The crustal-scale structural model that corresponds to models 1 is illustrated along a representative SSW–NNE oriented cross section (see Fig. 1b) down to 30 km depth (Fig. 4a). In the southwest, the cross section cuts the inverted southern basin margin and continues further through the basin centre along the salt structures to the NNE. Aside the legend shows the thermal conductivities that have been assigned to each layer for model 1. Figure 4b visualises the temperature distribution obtained for model 1 from the basin margin to the salt structures of the basin centre.

The isotherms are bent downward below the basin margin and upward at the basin centre, as can be seen below the 5 km depth level. This observation is even more distinct in a zoom in on the basin fill (Fig. 4c, d). These figures illustrate the impact of both the high thermal conductivity of the salt diapirs and the crust on the temperature

distribution down to 5 km depth. The temperatures at the 5 km depth level vary laterally across the basin and decrease towards the basin margin in the southwest by about 50°C. Highest temperatures are predicted at 2 km depth in the proximity of the most significant diapir in the basin centre, where the thickness maxima of the clastic overburden are largest above the salt diapirs. There, additional structural complexity comes from the salt rim synclines which are filled with up to 2,000 m weakly consolidated low conductive Tertiary clastics (Noack et al. 2010). Lowest temperatures occur at the basin margin, where the highly conductive crust comes close to the surface and no significant sedimentary cover is present. Consequently, heat can efficiently escape in these areas.

The lithosphere-scale structural model 2 is displayed in Fig. 5a down to the LAB along the same cross section as in Fig. 4. The scale bar of the legend shows in addition to the basin fill the conductivities for the refined crystalline crust and the mantle used in model 2. The configuration of the upper crust displays a thickening towards the basin margin in the SSW, whereas the thinning of the upper crust in the NNW is accompanied by a thickening of the lower crust (Fig. 5a). The base of the 1,300°C isotherm, acting as the lower boundary, is shallowest in the SW and varies

Fig. 4 a NNE–SSW oriented cross section through the 3D crustal-scale structural model with colour key for the assigned thermal conductivities. b Modelled temperatures along the same cross section for thermal model 1. c Zoom into the shallow part of the cross section down to 5 km. d Zoom in on modelled temperatures in b
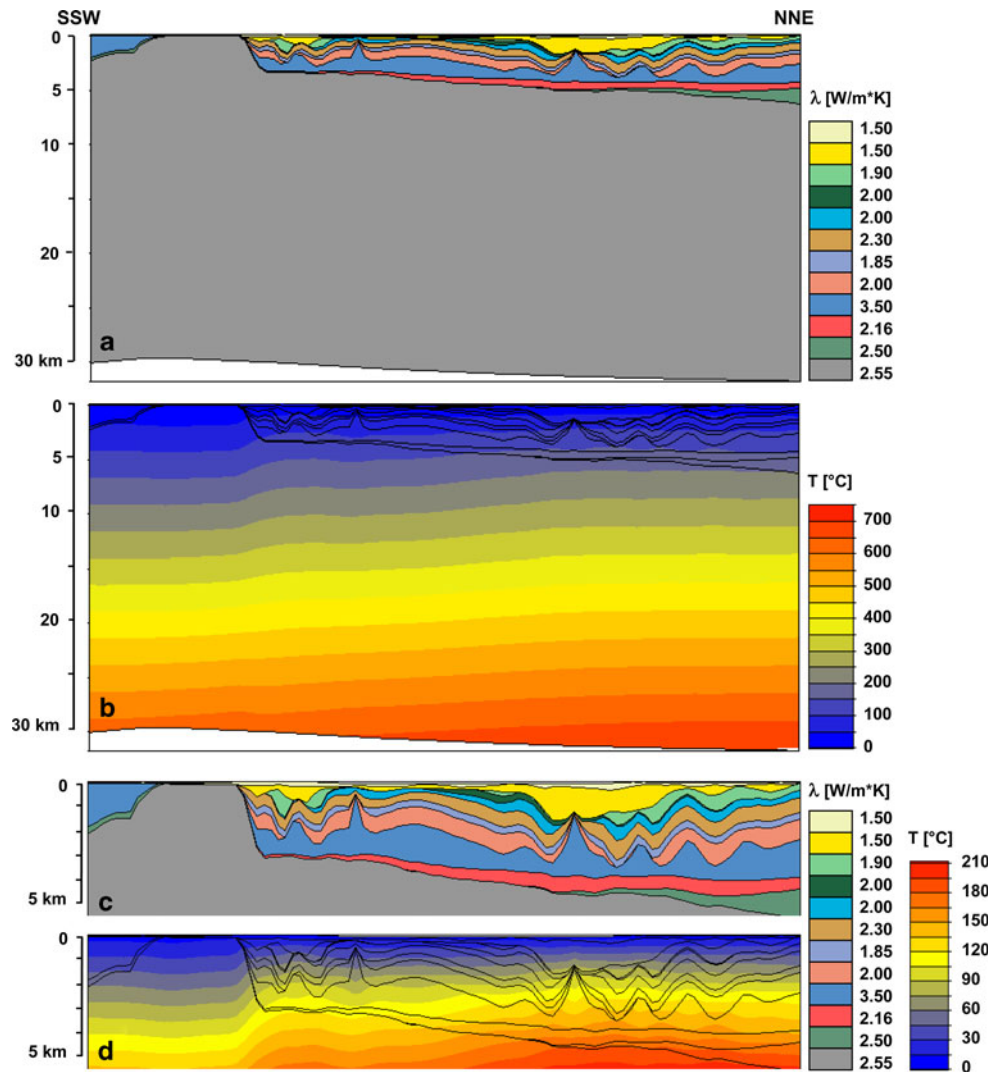
according to Fig. 5b. The 1,300°C isotherm is bent convex upward within the crustal thickening and bent softly downward towards the basin centre.

At the southern basin margin, where the upper crust is thickest and closest to the surface, no relevant insulating sediments overlying the crust are present. This configuration causes a mega chimney effect due to the very high thermal conductivity of the upper crust. In other words, the efficient heat transport to the surface leads to a loss of heat which is reflected by lower temperatures predicted down to about 20 km depth. In contrast, the increasing thickness of the overlying sediments towards the basin centre causes the storage of the heat below and hence increased temperatures in these areas.

Figure 6 shows the calculated temperature distribution for selected depth levels of both models, the crustal-scale 3D model 1 (a1–c1) and the lithosphere-scale model 2 (a2–c2). A comparison of all temperature maps shows a strong lateral variation of predicted temperatures across the study area with lower temperatures towards the southern basin

margin and higher temperatures in the basin area. This lateral variation in temperatures is controlled by the position and configuration of the underlying crust in interaction with the configuration of the Zechstein salt and the sediments.

The temperature maps at 3,000 m depth (Fig. 6a1, a2) cut the southern basin margin, Mesozoic sediments and salt structures within the basin area. The pattern of the temperature distribution is characterized by both a long-wavelength trend of increasing temperatures from the southern basin margin towards the basin centre and a short-wavelength trend in the deeper basin area. The long-wavelength pattern is caused by the interaction between the configuration of the crust and the sediments. The short-wavelength pattern results from the interaction between the configuration of the Zechstein salt and the overlying sediments. The latter is similar for both models.

Due to the high thermal conductivity of the crust, lowest temperatures of up to 70°C have been calculated at the southern basin margin for model 1. The temperatures

Fig. 5 a NNE–SSW oriented cross section through the 3D lithosphere-scale structural model with colour key for the assigned thermal conductivities. **b** Modelled temperatures along the same cross section for thermal model 2
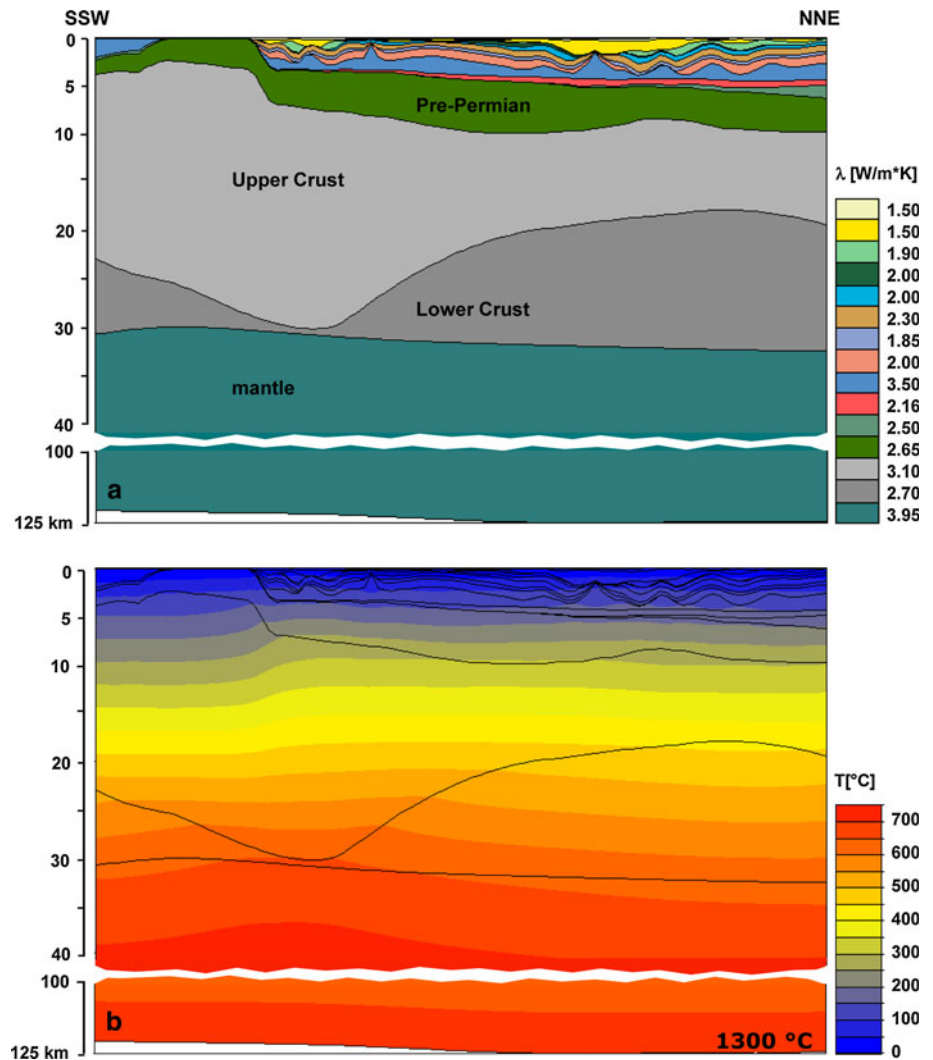
increase towards the basin centre to up to 140°C according to the cumulative thickness of the post-salt deposits which provoke a thermal blanketing effect in response to their low conductivity. Highest temperatures are predicted in the areas adjacent to the salt diapirs, where the surrounding low conductive sediments also cause thermal blanketing and the storage of the heat below.

For model 2, the configuration of the crust plays an important role for the temperature distribution. The reason is a higher heat input generated by the granites of the upper crust. Accordingly, a larger volume of upper crust contributes a larger amount of radiogenic heat. As almost the entire southern area of model 2 is characterized by an increased thickness of the upper crust, higher temperatures are also predicted in areas devoid of salt structures (Fig. 6a2). Apart from that, larger areas of increased temperatures are predicted around salt diapirs in the northern model area, triggered by the heat input of the thick underlying upper crust. Like in model 1, the lowest temperatures are predicted at the southern basin margin, but

their range between 100 and 120°C is distinctly warmer (by around 40°C) compared with model 1. Although the highest temperatures predicted for both models are in the same range (around 140°C), the comparison between both models indicates clearly that model 1 predicts lower temperatures than model 2 in those areas where the upper crust is thick.

The temperature maps at 6,000 m depth (Fig. 6b1, b2) cut pre-permian crust below the salt structures in the north-western part of the model. For both models, the pattern in the temperature distribution changes with increasing depth. In particular, the spatial correlation between the pattern of the temperature distribution and the thickness of the salt is only weakly expressed by a few cold spots beneath the most mature diapirs. In contrast, a more pronounced long-wavelength trend of the temperature pattern points to the increasing influence of the underlying crust. For model 1, the long-wavelength trend of increasing temperatures from the southern basin margin towards the basin centre correlates with the thickness distribution of the post-salt
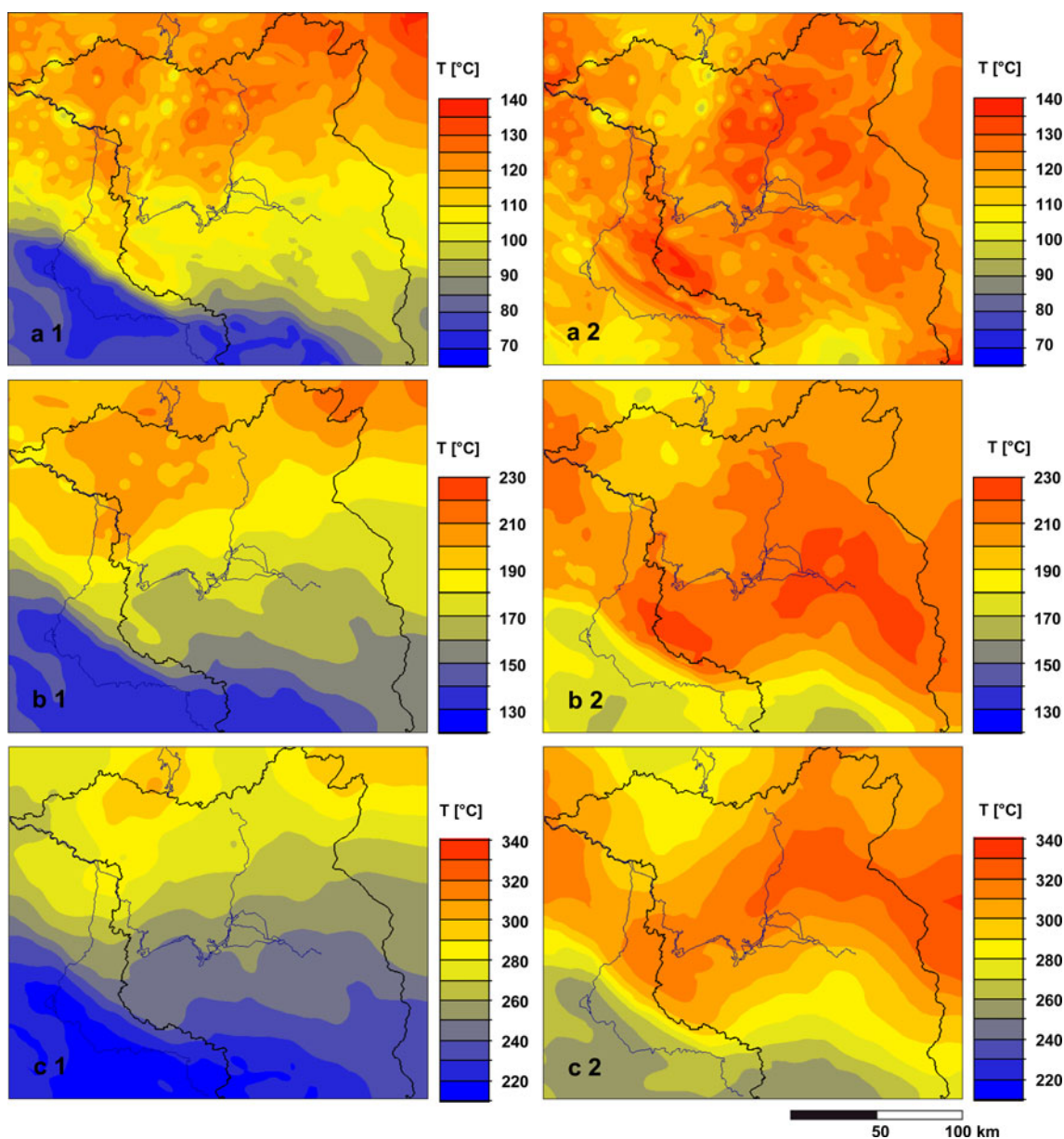
Fig. 6 Predicted temperatures in °C extracted from the 3D conductive thermal models: for model 1 (**a1–c1**) and model 2 (**a2–c2**) at the depth of 3,000 m (**a**), at 6,000 m (**b**) and at 10,000 m (**c**)

deposits. Accordingly, lowest temperatures of up to 150°C are predicted at the southern basin margin and highest temperatures of up to 210°C are predicted for the basin centre in the northern model area (Fig. 6b1). For model 2, the long-wavelength trend of increasing temperatures (Fig. 6b2) additionally correlates with the thickness maxima of the upper crust (see Fig. 5a). In the north-western area, where the upper crust is thinnest, lower temperatures are predicted (180–200°C) than in model 1 where the crust is homogeneous. Towards the southern and eastern area, the large thickness of the upper crust leads to a drastic increase in temperatures to up to 230°C in model 2. In all

temperature-depth maps, the lowest temperatures have been calculated for both models at the southern basin margin; there, the highly conductive crust is thickest and not covered by low conductive sediments. The lowest temperatures predicted for model 2 are warmer (160–190°C) than those predicted for model 1 (~150°C) in response to the higher value of radiogenic heat production assigned to the upper crust in model 2.

At the depth of 10,000 m (Fig. 6c1, c2), the influence of the salt structures is not evident any more in both models. The correlation between the sediments and the underlying crust is now expressed in a smooth long-wavelength pattern

of the temperature distribution. But similar to the temperature pattern at 6,000 m depth, the temperature distribution differs. For model 1, the temperature distribution is clearly influenced by the thickness of the post-salt deposits, whereas the temperature pattern of model 2 suggests an additional influence of the underlying crust. Again, lowest temperatures occur at the basin margin for both models. For the colder model 1, the lowest temperatures vary between 210 and 230°C, whereas for the warmer model, temperatures between 250 and 270°C are predicted. In response to the largest cumulative thickness of the overburden, the highest temperatures of up to 300°C have been modelled for model 1 in the northern model area. For model 2, the highest temperatures of up to 330°C clearly correlate spatially with the thickest upper crust in combination with a thick sediment fill.

To evaluate the results from the crustal-scale model 1 as well as the lithosphere-scale model 2, we test the validity of the models. Therefore, we extract the temperatures of both models for the respective coordinates and depths, where observed temperatures are available (Tables 3, 4). The comparison between temperature predictions of model 1 (blue line) and model 2 (green line) with observed temperatures (red triangles) show that both models reproduce observed temperatures well (Fig. 7a). Although the amount of temperature data is limited and thus also the statistical significance, the scatter of temperatures derived from different structural elements at different depth confirms this finding.

Nevertheless, model results indicate that model 1 is colder than model 2. For shallower depths (up to 2 km), the predicted temperatures of models 1 and 2 overestimate the observed temperatures slightly. This indicates that the chosen thermal conductivities are either too large or cooling due to moving groundwater may occur. Between 2 and 5 km, the wider scatter of observed temperatures (84 temperatures from 45 wells) reflects the larger variety of structural levels in which these values have been measured. Nevertheless, in this depth interval, the deviation between model predictions and observations is small for model 1, and larger for model 2. For model 1, 80% of the model predictions show deviation smaller than 10 K from observations, whereas for model 2 only 65% stay within this range. Thereby, distinctly overestimated temperatures deviate in the range between 10 and 20°C for model 2 (Tables 3, 4). This comparison is only valid down to 7 km, as no temperatures were available below this depth level.

Sensitivity with respect to thermal properties

A wide range of values for rock properties is measured in wells of the NEGB due to the natural petrophysical heterogeneity of rocks (Čermák et al. 1982; Norden and Förster 2006). As described before, the first dataset includes parameter values after Bayer et al. (1997) for the layers of the basin fill, in particular average values of thermal conductivity. To consider the range of lithological variation we test a second dataset, which we assign to the crustal-scale model 3. This dataset includes recently measured properties on rocks taken from wells of the NEGB (Table 1).

Values for radiogenic heat production of the units for the basin fill are based on data determined by log analysis or drill cores by Norden and Förster (2006). Thermal conductivities of the Quaternary and Tertiary units and the Zechstein salt are assigned according to a study of Norden et al. (2008). For the Mesozoic strata (Upper Cretaceous—Buntsandstein), we use average bulk thermal conductivities calculated from a thermal conductivity profile of the well Stralsund 1/85 by Fuchs and Förster (2010). Thermal conductivities for the Sedimentary Rotliegend and the Permo-Carboniferous Volcanics are based on data determined on drill cores from Norden and Förster (2006).

The comparison of both datasets, as illustrated in Table 1, reveals that the measured values for the thermal conductivities exceed the ones used by Bayer et al. (1997). This is especially the case for the Upper Cretaceous, the Lower Cretaceous and the Jurassic, where measured values are one-third higher than the conductivities after Bayer et al. 1997. Likewise, the thermal conductivity for the Zechstein salt is about 1 W/m K higher. In contrast, the measured values for the radiogenic heat production show rather small differences between the two datasets. Since these thermal properties are valuable real observations, we run several simulations for model 3 using the same homogeneous configuration of the crust as used for model 1 but varied thermal conductivities to assess the influence on the modelling results.

Modelling results for model 3 show that predicted temperatures do not reproduce the observed temperatures in wells in a similar manner like models 1 and 2 (Fig. 7a). Although, for the upper 2 km the model fits the observed data better than models 1 and 2, the predicted temperatures are lower than observed for depth levels between 2 and 7 km. Between 5 and 7 km depth, this mismatch reaches up to about 40 K. This difference between model prediction and observation is 30 K larger compared to model 1.

A stepwise variation of thermal properties for the upper crust (λ to 3.3 W/m K and S to 3.0e−6 W/m^3) and for the Permo-Carboniferous Volcanics (S to 3.4e−6 W/m^3) within a reasonable range, leads to an increase in temperatures, but is not sufficient to reproduce the observations. Likewise, increasing the heat flow to 35–40 mW/m^2 as suggested by Norden et al. (2008) leads to generally higher temperatures but these are still too low to reproduce the observations.

Fig. 7 a Comparison of measured and predicted temperatures: for models 1, 2 and 3. **b** Largest difference between observed and modeled temperatures for the wells of model 2 superimposed on the isopach map of the Zechstein salt
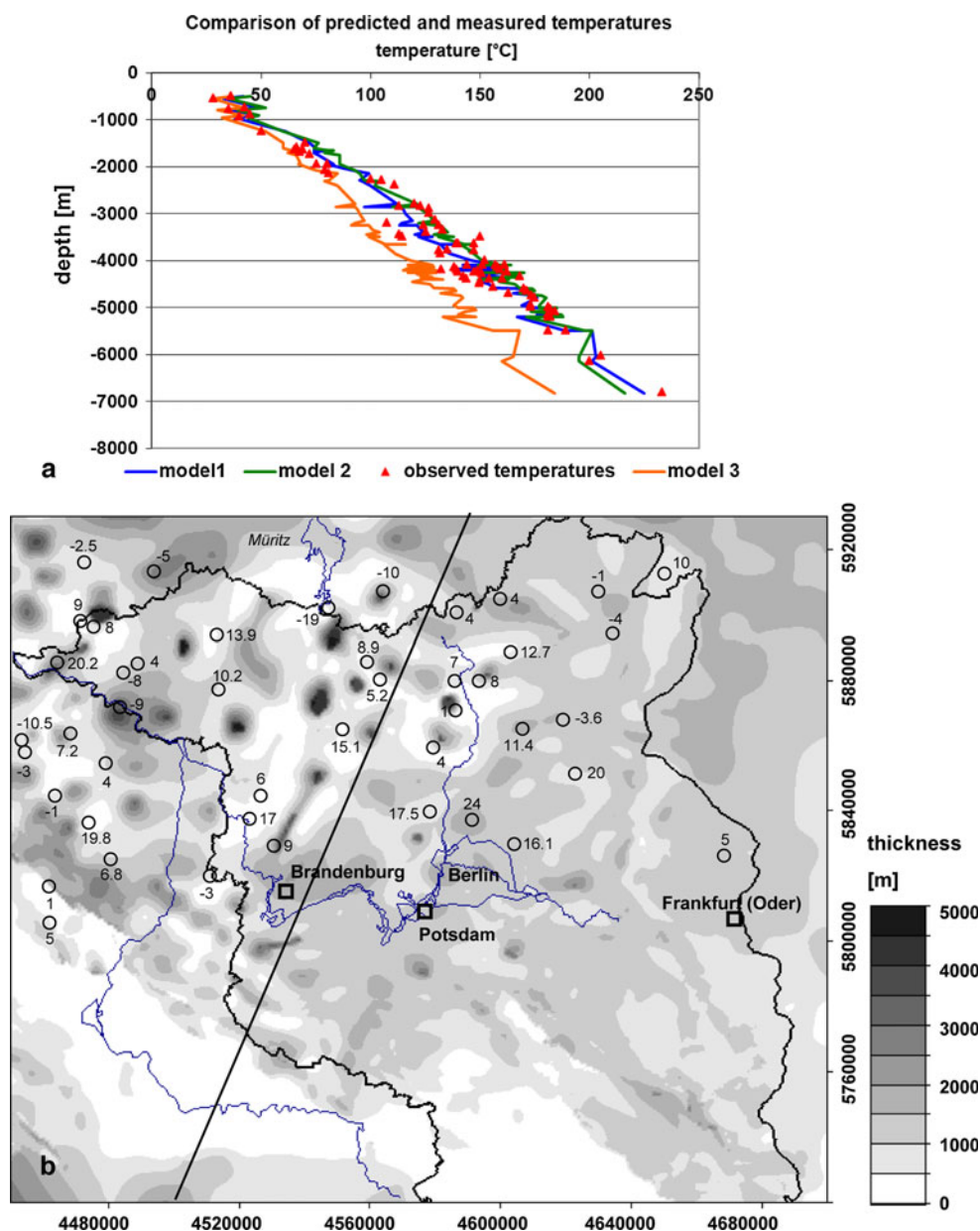
Discussion

The comparison between predicted and measured temperatures (Förster 2001) of the different thermal models shows that using thermal parameters after Bayer et al. (1997) as adopted for the crustal-scale model 1 and the lithosphere-scale model 2 leads to comparatively small deviations between predicted and observed temperatures. A larger misfit between model predictions and observations occurs in the upper 2 km for both models (Tables 3, 4; Fig. 7b). Possible reasons for this deviation could be related to limitations in model resolution as connected to extrapolations in areas where no structural data were available. This is especially the case for locations in the periphery of the model.

Likewise, simplified model assumptions such as laterally uniform geological units do not consider the heterogeneity of depositional sequences, both vertically and laterally. This also could result in erroneous predictions in areas where such lithological heterogeneities are present.

Furthermore, the observed temperatures of the shallow temperature field above the Zechstein salt may be additionally influenced by cooling effects due to moving groundwater in the permeable layers.

How far the temperatures predicted for the southern part of the model are valid remains uncertain as no temperature observations covering this area were available.

For the temperature field between 2 and 5 km depth, the deviation between model prediction and observation is

small for model 1 and partly larger for the warmer model 2 (Tables 3, 4; Fig. 7b). To figure out the reason for this larger deviation we compare the temperature predictions of model 1 (Fig. 8a) and model 2 (Fig. 8b) with the thickness map of the upper crust. The comparison reveals that model 2 predicts much higher temperatures compared with model 1 in the region of the model area where the upper crust is thickened. This is the case in the east at the south-western basin margin, where the predicted temperatures in model 1 are too cold, whereas model 2 overcomes the misfit with the observations. However, the higher heat input from the thickened upper crust also results in partly too high temperatures that deviate from observations by about 20 K (Fig. 8b) in the eastern part of the model area. The over-estimation of temperatures could result from an overesti-mation of the radiogenic heat production in the upper crust as no spatial variations in crustal composition are resolved in the model. How far the overestimation is caused by the assumption of a purely conductive heat transport, needs to be tested further, as studies of coupled fluid and heat flow in the NEGB give more than indications for the presence of a convective fluid system in the subsurface (Cacace and Scheck-Wenderoth 2010). Likewise, the cooler observa-tions in these areas could be related to cooling effects occurring due to forced convective processes as described by Kaiser et al. (2011).

Nevertheless, our studies show that the average values of thermal conductivity as used in models 1 and 2 repro-duce observed temperatures reasonably well. This indicates that the chosen values may represent "effective" thermal conductivities that are different from real conductivities measured on the rock samples. The temperatures predicted by model 3 remain distinctly colder than in models 1 and 2.

This is not surprising as most values of the thermal con-ductivities are larger for the sedimentary units in this model. A stepwise variation of thermal properties has shown that the shallow temperature predictions are not very sensitive to changes in radiogenic heat production, but highly sensitive to changes in the thermal conductivities of the respective sedimentary layers. Thus, the large deviation between observed and predicted temperatures below 2 km for model 3 seems to be related to the very high thermal conductivities assigned. This effect implies three conclu-sions: (1) the assumption of a uniform horizontal distri-bution of conductivities does not reflect the heterogeneity of the respective layers. These conclusions were also dis-cussed in the studies of Ollinger et al. (2010), who obtain a better fit with observed temperatures by assuming a non-uniform horizontal distribution of conductivities and by calculating optimized conductivities for individual wells. (2) The possible influence of heat transport processes due to deep circulating fluids is not sufficiently taken into account. Cacace and Scheck-Wenderoth (2010) assume that positive heat flow anomalies at the surface, resolved in the study of Norden et al. (2008), could result from deep circulating fluids transporting heat from the basement to the surface. This assumption is confirmed by studies of Kaiser et al. (2011) who show that the formation of thermal convective cells leads to positive small-wavelength thermal anomalies in certain areas within the NEGB. Such phe-nomena could also explain the underestimated temperatu-res predicted by model 3. (3) The simple vertical model resolution which is defined by the number of layers resolved in the model may not account for vertical anisotropy. The latter may exist in response to the presence of thin intercalated layers of reduced thermal conductivity.
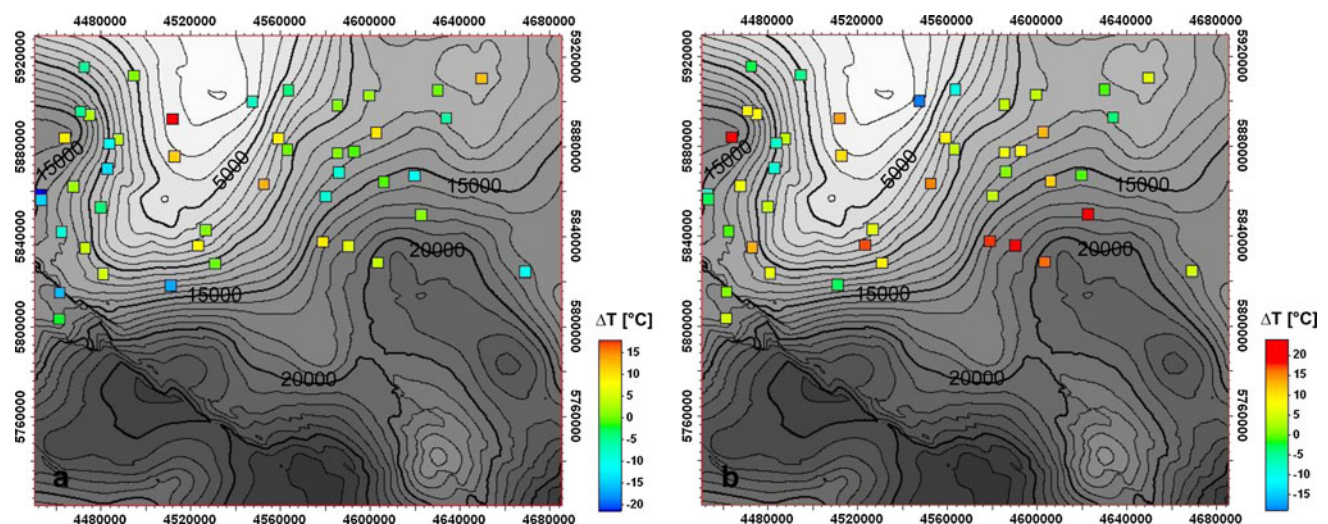

Fig. 8 Thickness of the upper crust for the model area with location of wells where measured temperatures are available. Coordinates are Gauss Krüger zone 4. *Coloured squares* represent difference between temperatures and predictions for **a** the crustal-scale model 1 and **b** the lithosphere-scale model 2

Such deposits may be responsible for increased temperatures due to the storage of the heat below these layers. Studies from Mottaghy et al. (2011) on a small scale model reveal the strong sensitivity of the temperature field to thermal conductivity by means of the upper and lower limit of temperature profiles resulting from varying thermal conductivities. (4) Furthermore, our approach does not take into account the possible influence of faults which may provide pathways for an upward migration of warm fluids within the model area. Lampe and Person (2002) showed in their studies on advective cooling within the Upper Rhinegraben (Germany) that fault-related factors can play a major role in determining the geothermal regime. Moreover, Yousafzai et al. (2010) indicate in their studies on the Himalayan foreland basin that hydrochemical signatures of groundwater samples such as water and reservoir temperatures calculated for spring waters point to origin from deep horizons. They suggest that the remarkable proximity of thermal and hydrochemical anomalies to major faults are caused by waters ascending along these faults from greater depth. Likewise, the rise of deep high-salinity groundwater along tectonic fracture zones has been described for the western area of Apennine ridge by Petitta et al. (2011); there, these ascending saline brines mix with shallow groundwater in Quaternary deposits filling depressed areas. (5) The assigned thermal conductivities for the Mesozoic layers have been derived from only one location, which may not be representative for the entire basin.

The use of measured thermal properties for the crustal-scale model 3 resulted in a large deviation between predicted and observed temperatures. The reason for this strong deviation of predicted temperatures could be related to the assumption of a homogeneous crust producing insufficient heat in certain areas of model 3. Therefore, in a stepwise variation, we have tested how much heat would be required at the level of the crust-mantle boundary to match the data. Our studies show that only a rather high heat flow of 50 mW/m^2 would reproduce the observed temperatures for the model with measured properties. Such a high heat flow at the Moho is in conflict with the general consensus (Huenges 2010). Accordingly, the heat flow from the mantle should vary in the range of 20–40 mW/m^2, where no anomalous hot zones at the base of the European crust are suggested. In addition, more recent results (Cacace et al. 2010) indicate that the heat flow at the Moho cannot be assumed to be laterally uniform. Nevertheless, our results suggest that there may be more heat entering the crust at its base than considered in model 3. An alternative way of increasing the heat input from the crust and mantle would be a differentiated crust as considered in model 2 in concert with a larger temperature at the lithosphere asthenosphere boundary. Sensitivity analyses testing these

scenarios proved that neither using a crustal differentiation nor increasing the basal temperature to 1,400°C were sufficient to reproduce the observations.

Conclusions

We show that the choice of both different configurations of the lithosphere and thus different lower boundary conditions, as well as of different thermal properties strongly influence the results of 3D thermal modelling. For the lower boundary of the models, we test two different model configurations, a fixed heat flow at the Moho and an isothermal boundary of 1,300°C at the LAB. Both, the 3D crustal-scale model as well as the 3D lithosphere-scale model of the steady-state conductive thermal field are able to reproduce observed temperatures, which indicates that conductive transport is the dominant mechanism of heat transfer on a basin scale.

Under the simplified assumption of a homogeneous crust, the crustal-scale model 1 using a constant heat flow of 30 mW/m^2 at the Moho leads to temperature predictions which largely reproduce observed temperatures. The more appropriate lithosphere-scale model 2 generates higher temperatures than model 1 due to its differentiated lithosphere and the related heat input at the base of the Permian to Cenozoic deposits. Although model 2 partly overestimates the temperature observations, the results are considered to be more realistic, since the model is consistent with temperature, deep seismic and gravity observations. Obviously, the chosen thermal parameters (Bayer et al. 1997) for the stratigraphic layers resolved in the model represent reasonable average values. However, these values may not correspond to the specific thermal properties measured on rock samples of these units.

Model 3 shows a less good correlation between predicted and observed temperatures below 2 km depth. Although below 2 km depth, the trend of the temperature distribution is similar to those of models 1 and 2, model 3 predicts colder temperatures compared with the observations. Moreover, the increase in temperatures predicted by model 3 using the differentiated lithosphere, does not overcome the misfit with the observations.

In summary, our results suggest that the thermal regime in the Brandenburg area is mainly influenced by heat conduction, but there are also indications for the presence of moving fluids in restricted areas. The predicted temperature distribution itself is strongly controlled by two major influencing factors: (1) Configuration of the lithosphere and the chosen lower thermal boundary condition. (2) The effective thermal properties which according to our results are characterized by smaller values than those determined on rock samples.

References

Bayer U, Scheck M, Koehler M (1997) Modeling of the 3D thermal field in the northwest German Basin. Geol Rundsch 86:241–251

Beer H (1996) Temperaturmessungen in Tiefbohrungen - Repräsentanz und Möglichkeit einer näherungsweisen Korrektur. Brandenburgische Geowissenschaftliche Beiträge 3:28–34

Beer H, Hurtig E (1999) Das geothermische Feld in Brandenburg. Brandenburgische Geowissenschaftliche Beiträge 6:57–68

Benek R, Kramer W, McCann T, Scheck M, Negendank JFW, Korich D, Huebscher HD, Bayer U (1996) Permo-carboniferous magmatism of the Northeast German Basin. Tectonophysics 266:379–404

Cacace M, Scheck-Wenderoth M (2010) Modeling the thermal field and the impact of salt structures in the North East German Basin. World Geothermal Congress, Bali, Indonesia

Cacace M, Kaiser BO, Lewerenz B, Scheck-Wenderoth M (2010) Geothermal energy in sedimentary basins: what we can learn from regional numerical models. Chemie der Erde-Geochemistry 70:33–46

Čermák VH, Huckenholz HG, Rybach L, Schmid R, Schopper JR, Schuch M, Stöffler D, Wohlenberg J (1982) Physical properties of rocks. In: Augenheister G (ed) Landolt-Börnstein. New series. Springer, Berlin, Heidelberg, New York, pp 1–373

Förster A (2001) Analysis of borehole temperature data in the Northeast German Basin: continuous logs versus bottom-hole temperatures. Pet Geosci 7:241–254

Fowler CMR (1996) The solid earth. Cambridge University Press, Cambridge

Fuchs S, Förster A (2010) Rock thermal conductivity of Mesozoic geothermal aquifers in the Northeast German Basin. Chemie Der Erde-Geochemistry 70:13–22

Hofmeister AM (1999) Mantle values of thermal conductivity and the geotherm from phonon lifetimes. Science 283:1699–1706

Huenges E (ed) (2010) Geothermal energy systems. WILEY-VCH, Weinheim

Hurtig E (1975) Untersuchungen zur Wärmeflußverteilung in Europa. Gerlands Beiträge zur Geophysik 84:247–260

Hurtig E, Oelsner Ch (1979) The heat flow field on the territory of the German Democratic Republik. In: Cermak V, Rybach L (eds) Terrestrial heat flow in europe. Springer, Berlin, pp 186–190

Hurtig E, Čermák V, Haenel R, Zui V (1992) Geothermal Atlas of Europe. H Haak Verlagsgesellschaft, Gotha

Kaiser BO, Cacace M, Scheck-Wenderoth M, Lewerenz B (2011) Characterization of main heat transport processes in the Northeast German Basin: constraints from 3-D numerical models. Geochem Geophys Geosyst 12:17. doi:10.1029/2011GC003535

Lampe C, Person M (2002) Advective cooling within sedimentary rift basins—application to the Upper Rhinegraben (Germany). Mar Petrol Geol 19:361–375

Maystrenko YP, Scheck-Wenderoth M (2011) Shallow and deep controls on the thermal structure of basins—predictions from data-based large-scale 3D models. In: Poster, EGU general Assembly 2011, vol 13, EGU2011-3598

Mottaghy D, Pechnig R, Vogt C (2011) The geothermal project Den Haag: 3D numerical models for temperature prediction and reservoir simulation. Geothermics 40:199–210

Noack V, Cherubini Y, Scheck-Wenderoth M, Lewerenz B, Höding T, Simon A, Moeck I (2010) Assessment of the present-day thermal field (NE German Basin)-inferences from 3D modelling. Chemie Der Erde-Geochemistry 70:47–62

Norden B, Förster A (2006) Thermal conductivity and radiogenic heat production of sedimentary and magmatic rocks in the Northeast German Basin. AAPG Bull 90:939–962

Norden B, Förster A, Balling N (2008) Heat flow and lithospheric thermal regime in the Northeast German Basin. Tectonophysics 460:215–229

Ollinger D, Baujard C, Kohl T, Moeck I (2010) Distribution of thermal conductivities in the Gross Schonebeck (Germany) test site based on 3D inversion of deep borehole data. Geothermics 39:46–58

Ondrak R, Wenderoth F, Scheck M, Bayer U (1998) Integrated geothermal modeling on different scales in the Northeast German basin. Geol Rundsch 87:32–42

Petitta M, Primavera P, Tuccimei P, Aravena R (2011) Interaction between deep and shallow groundwater systems in areas affected by Quaternary tectonics (Central Italy): a geochemical and isotope approach. Environ Earth Sci 63:11–30

Scheck M (1997) Dreidimensionale Strukturmodellierung des Nordostdeutschen Beckens unter Einbeziehung von Krustenmodellen (Dissertation Thesis, Freie Universität Berlin). Scientific Technical Report STR97/10, pp 1–126

Scheck M, Bayer U (1999) Evolution of the Northeast German Basin—inferences from a 3D structural model and subsidence analysis. Tectonophysics 313:145–169

Scheck M, Bayer U, Lewerenz B (2003) Salt redistribution during extension and inversion inferred from 3D backstripping. Tectonophysics 373:55–73

Scheck-Wenderoth M, Maystrenko Y (2008) How warm are passive continental margins? A 3-D lithosphere-scale study from the Norwegian margin. Geology 36:419–422

Scheck-Wenderoth M, Krzywiec P, Zühlke R, Maystrenko Y, Froitzheim N (2008) Permian to cretaceous tectonics. In: McCann T (ed) The geology of central Europe, vol 2., Mesozoic and CenozoicGeological Society of London, London, pp 999–1030

Schössler KS, Schwarzlose J (1959) Geophysikalische Wärmeflussmessungen. Freiberger Forsch-H. C75, Leipzig

Schwab G (1985) Paläomobilität der Norddeutsch-Polnischen Senke. Akademie der Wissenschaften der DDR, Dissertation B, Berlin

Turcotte DL, Schubert G (2002) Geodynamics, 2nd edn. Cambridge University Press, Cambridge

Yousafzai A, Eckstein Y, Dahl PS (2010) Hydrochemical signatures of deep groundwater circulation in a part of the Himalayan foreland basin. Environ Earth Sci 59:1079–1098